Disorders of the Nervous System

Circadian and Brain State Modulation of Network Hyperexcitability in Alzheimer's Disease

Rosalind Brown,[1,*] Alice D. Lam,[2,3,*] Alfredo Gonzalez-Sulser,[1,*] Andrew Ying,[1] Mary Jones,[1] Robert Chang-Chih Chou,[1] Makis Tzioras,[1] Crispin Y. Jordan,[1] Izabela Jedrasiak-Cape,[1] Anne-Laure Hemonnot,[4] Maurice Abou Jaoude,[2,3] Andrew J. Cole,[2,3] Sydney S. Cash,[2,3] Takashi Saito,[5] Takaomi Saido,[5] Richard R. Ribchester,[1] Kevan Hashemi,[6] and Iris Oren[1]

[1]Centre for Discovery Brain Sciences, University of Edinburgh, Edinburgh, EH8 9JZ, United Kingdom, [2]Epilepsy Division, Dept of Neurology, Massachusetts General Hospital, Boston, MA 02214, [3]Harvard Medical School, Boston, MA 02214, [4]Université de Montpellier, Montpellier, 34000 France, [5]Laboratory for Proteolytic Neuroscience, RIKEN Center for Brain Science, Saitama, 351-0198 Japan, [6]OpenSource Instruments Inc, Watertown, MA 02472

Abstract

Network hyperexcitability is a feature of Alzheimer' disease (AD) as well as numerous transgenic mouse models of AD. While hyperexcitability in AD patients and AD animal models share certain features, the mechanistic overlap remains to be established. We aimed to identify features of network hyperexcitability in AD models that can be related to epileptiform activity signatures in AD patients. We studied network hyperexcitability in mice expressing amyloid precursor protein (APP) with mutations that cause familial AD, and compared a transgenic model that overexpresses human APP (hAPP) (J20), to a knock-in model expressing APP at physiological levels (APP$^{NL/F}$). We recorded continuous long-term electrocorticogram (ECoG) activity from mice, and studied modulation by circadian cycle, behavioral, and brain state. We report that while J20s exhibit frequent interictal spikes (IISs), APP$^{NL/F}$ mice do not. In J20 mice, IISs were most prevalent during daylight hours and the circadian modulation was associated with sleep. Further analysis of brain state revealed that IIS in J20s are associated with features of rapid eye movement (REM) sleep. We found no evidence of cholinergic changes that may contribute to IIS-circadian coupling in J20s. In contrast to J20s, intracranial recordings capturing IIS in AD patients demonstrated frequent IIS in non-REM (NREM) sleep. The salient differences in sleep-stage coupling of IIS in APP overexpressing mice and AD patients suggests that different mechanisms may underlie network hyperexcitability in mice and humans. We posit that sleep-stage coupling of IIS should be an important consideration in identifying mouse AD models that most closely recapitulate network hyperexcitability in human AD.

Key words: Alzheimer's disease; circadian cycle; epilepsy

Significance Statement

It is increasingly recognized that Alzheimer's disease (AD) is associated with hyperexcitability in brain networks. Brain network hyperexcitability is also reported in several rodent models of AD. We studied the signatures of this hyperexcitability in two rodent models of AD as well as AD patients. Network hyperexcitability was prevalent in a transgenic model of AD but was absent in a rodent model that is considered to be more physiologic. Moreover, while network hyperexcitability was coupled to rapid eye movement (REM) sleep in transgenic mice, hyperexcitability occurred in non-REM (NREM) sleep in AD patients. We suggest that brain state coupling of hyperexcitability can be used as a method for screening animal models of AD.

Introduction

An increased incidence of seizures in Alzheimer's disease (AD) is indicative of an underlying network hyperexcitability (Hesdorffer et al., 1996; Amatniek et al., 2006; Lozsadi and Larner, 2006; Vossel et al., 2013; Cretin et al., 2016). Interictal spikes (IIS) are also seen in a high proportion of AD patients without a history of clinical seizures (Vossel et al., 2016). Nonictal network hyperactivity has also been detected by means of fMRI in individuals at risk of developing dementia, for example in people carrying the APOE4 allele (Bookheimer et al., 2000; Filippini et al., 2009), with other genetic predictors of AD (Quiroz et al., 2010) and also in patients with mild cognitive impairment (MCI), a diagnosis which is considered to be a prodromal stage of AD (Dickerson et al., 2005). Network hyperexcitability and seizure activity appear at early stages of the disease and have been suggested to be predictors of accelerated cognitive decline (Amatniek et al., 2006; Vossel et al., 2013; Cretin et al., 2016; Vossel et al., 2016).

Network hyperexcitability has also been reported in numerous mouse models of AD pathology (Palop et al., 2007; Minkeviciene et al., 2009; Busche et al., 2012; Šišková et al., 2014; Kazim et al., 2017), with the aberrant activity being a feature that occurs in advance of plaque deposition (Busche et al., 2012; Bezzina et al., 2015). These phenomenological similarities have led to the suggestion that these animal models can provide a tool by which to study network hyperexcitability in human AD (Palop and Mucke, 2016).

Aberrant network activity could in itself contribute to neurodegeneration and cognitive dysfunction in AD pathology (Cirrito et al., 2005; Bero et al., 2011; Busche and Konnerth, 2015; Wu et al., 2016). Reducing network hyperexcitability has been shown to ameliorate cognitive dysfunction in both patients and animal models (Bakker et al., 2012; Sanchez et al., 2012; Haberman et al., 2017), and to attenuate $A\beta$ pathology (Yuan and Grutzendler, 2016). Hence, targeting network hyperexcitability has

been suggested as a novel therapeutic avenue for AD. However, studying this therapeutic avenue by means of animal models (Sanchez et al., 2012) requires a deeper understanding of the shared features of network hyperexcitability between AD patients and animal models.

Expression of epileptiform activity frequently exhibits a circadian pattern and shows preferential activation with specific brain states in a range of epilepsies (Quigg, 2000; Ng and Pavlova, 2013; Sedigh-Sarvestani et al., 2015). Circadian dysfunction and sleep disruption are common features of AD and are also considered as early features of disease pathogenesis (Musiek et al., 2015; Mander et al., 2016; Musiek et al., 2018). Two recent papers have reported modulation of epileptiform activity by circadian cycle and brain state in transgenic AD models. Epileptiform activity was more prevalent in daylight conditions, and was suggested to occur primarily during rapid eye movement (REM) sleep (Born et al., 2014; Kam et al., 2016). If epileptiform activity is modulated by circadian cycles and/or brain state in AD patients, it is possible that this might contribute to the reported circadian alterations and sleep dysfunction. In line with this, it has recently been shown that interictal activity in AD patients is highly prevalent during sleep (Vossel et al., 2016; Horváth et al., 2017; Lam et al., 2017). The modulation of ictal related activity by brain state points to a distinguishing feature that could be used to (1) uncover distinct mechanisms underlying hyperexcitability, and (2) ascertain the translational utility of specific animal models in studying network hyperexcitability. To this end, the present study aimed to investigate circadian and brain state modulation of network hyperexcitability in two rodent models of AD of differing etiology: one in which human amyloid precursor protein (hAPP) is overexpressed and one in which APP is expressed at endogenous levels. In order to shed light on the translational utility of rodent AD models for studying network hyperexcitability in human AD, we further examined sleep-stage modulation of epileptiform activity in two patients with AD, using recordings from intracranial electrodes placed directly adjacent to the hippocampus.

Materials and Methods

Animals and animal maintenance

All animal procedures were performed in accordance with the University of Edinburgh animal welfare committee regulations and were performed under a United Kingdom Home Office project license.

Heterozygous mice $(+/-)$ expressing hAPP with the KM670/671NL (Swedish) and V717F (Indiana) mutations on a PDGFβ promoter (J20; Mucke et al., 2000) were bred by crossing J20 $+/-$ (i.e. animals are heterozygous) males with C57Bl6J females. Experiments used J20 $+/-$ ($n = 21$) and J20-/- ($n = 8$) wild-type (WT) littermate controls. The mean age of J20 animals was five months (range: 3.3–6.5 months).

Homozygous knock-in mice expressing APP KM670/671NL (Swedish) and APP I716F (Iberian) mutations (APP$^{NL/F}$; Saito et al., 2014) were back-crossed onto C57Bl6J strain for at least three generations and were >99.8% cogenic with C57Bl6J. Experiments used APP$^{NL/F}$ $+/+$ ($n =$

Copyright © 2018 Brown et al.

20) and age-matched nonlittermate C57Bl6J WT controls ($n = 15$). Animals were either eight or 12 months of age.

Both male and female mice were used. Mice were kept on a 7/19 h light/dark cycle in standard, open cages. Mice were group-housed before surgery and were housed individually postsurgery and during telemetry data acquisition.

Surgery and data acquisition

A subdural intracranial electrocorticogram (ECoG) recording electrode was positioned in the cortex overlying the hippocampus (coordinates x: -2.25; y: -2.46). A reference electrode was implanted either in the skull of the contralateral hemisphere, or above the cerebellum. Electrodes were either bare wire, or skull screws. An EEG transmitter (A3028B, Open Source Instruments) was implanted on the back of the animal subcutaneously. Animals were left to recover for at least 24 h after surgery before the commencement of telemetry data acquisition. Telemetric ECoG data were acquired for ~3 d from each animal. Recording was either conducted continuously between days 1 and day 3 after surgery, or day 1, followed by day 5 to day 6.

ECoG data were acquired using an Opensource Instruments data acquisition system at 512 sps as previously described (Chang et al., 2011).

Video data were acquired using a Basler acA1300-60gm GigE camera sampling at 10 fps, or a Logitech C270 HD webcam sampling at 5 fps. Video was acquired during the daylight hours.

ECoG data processing

The raw ECoG data were analyzed using custom written Tcl and C processors. ECoG data were analyzed in 8-s intervals. For each interval we extracted measures of data loss, spike count, δ power (0.1–3.9 Hz) and θ power (4–12 Hz). We defined intervals in which data loss exceeded 20% of samples as "lossy" intervals. Intervals in which δ power exceeded 0.16 mV^2 were classified as artifacts. Lossy and artifact intervals were excluded.

IIS in rodent ECoG were detected as follows. Each 8-s interval of EEG was treated as a two-dimensional path. One dimension is voltage, which was normalized by dividing by the mean absolute step size of the voltage in the 8-s interval. The mean absolute step size is the sum of the absolute changes in voltage from one sample to the next, divided by the number of samples. For an 8-s interval, the number of samples would be 4096 and a typical mean absolute step size for mouse EEG is around 12 μV. The other dimension is time, which was normalized by dividing by the sample period. The spike-finder proceeds along this EEG path in steps. With each step, it moves to the nearest sample on the path ahead. Whenever the spike-finder steps past one or more samples, it classifies these samples as an aberration in the path. Solitary aberrations larger than 20 mean absolute step sizes are classified as IIS. A series of IIS in which single spikes were separated by <78 ms (40 samples) were treated as a burst event and counted as one IIS event within the 8-s interval.

For each J20 animal, the false positive rate of IIS detection was determined by randomly hopping through 100 8-s intervals identified by the processor as containing IIS and scoring them as true or false positives. The animal was excluded from analysis if the false positive rate exceeded 10%. One animal was excluded from analysis on this basis. In the remaining animals, the false positive rate ranged from 0% to 6% (mean false positive rate: 1.9%).

We observed that lossy and artifactual intervals resulted from movement and external sources of interference. We could not exclude the possibility that these events are nonrandomly distributed across the 24-h cycle. Nonrandom exclusion of intervals would impact the evaluation of coupling of IIS. We thus set a criterion: if >5% of all 8-s intervals were excluded due loss or artifact, the animal was excluded from calculations of coupling of IIS to circadian cycles, sleep-wake, and θ/δ. Two J20 animals which were included in Figure 1 were excluded from data reported in Figures 2–4 on this basis (25% and 16% of 8-s intervals excluded in these animals).

Video analysis

Video data were manually scored to classify periods as "sleep" or "wake." Based on previous reports, sustained inactivity $\geq$40 s was classified as sleep, while stationary periods <40 s and periods of movement were classified as wake (Pack et al., 2007). Postural shifts during sleep epochs did not break sleep epochs.

Immunohistochemistry and imaging

Animals were killed by transcardial perfusion with *N*-methyl-D-glucamine (NMDG)-based saline solution (92 mM NMDG, 2.5 mM KCl, 1.25 mM NaH$_2$PO$_4$, 20 mM HEPES, 30 mM NaHCO$_3$, 25 mM glucose, 10 mM MgCl$_2$, 0.5 mM CaCl$_2$, and sucrose to adjust osmolarity to 315–330 mOsm). Brains were postfixed with 4% paraformaldehyde for 24 h then washed and stored in PBS. Samples were put in 50% or 30% sucrose, PBS solution and 50% OCT solution for 24 h before cutting, then placed in the same solution and cut using a freezing microtome.

Fifty-micrometer sections were stored in PBS at 4°C. Slices were presoaked with 5% rabbit normal serum (RNS; Vector S-5000), 0.2% Triton X-100, PBS solution for 30 min at room temperature (RT), followed by incubation with 3% RNS, 0.2% Triton X-100, anti-choline acetyltransferase (ChAT; 1:500, Millipore #AB144P, RRID: AB_2079751), PBS solution for 48 h at 4°C. The sections were washed three times with PBS 0.2% Triton X-100 for 5min each and then incubated in 3% RNS, anti-goat biotinylated (1:200), DAPI (1:5000, Sigma D9542-1MG), PBS solution for 1 h at RT. After 3 PBS 0.2% Triton X-100 washings of 5min each, the sections were incubated with ABC reagent (Vectastain PK-6105 kit) prepared half an hour before using and stored in foil at 4°C containing 0.1% of A, 0.1% of B, 0.01% Triton X-100, PBS for 1 h at RT. After six PBS washings of 10 min each, the sections were put in three 3'-diaminobenzidine (Sigma D5905-50TAB), 0.02% CoCl$_2$ (1% wt/vol), 0,04% (NH$_4$)$_2$Ni(SO$_4$)$_2$ (1% wt/vol) dH$_2$0 solution for 30 min at 4°C over agitation. Then stained by adding 1.2% of fresh 1% H$_2$0$_2$ per slice for 10–20 s until the slice darkened. The slices were then transferred and washed in PBS, six times for 10 min each, mounted on a slide and dried for 30 min at 50°C then

finally covered with Mowiol Embedding Medium and coverslips. Slides were stored at RT.

Imaging was performed on a Zeiss AX10 microscope using StereoInvestigator Software with a 5x/0.16 (420630-9900) apochromat air objective. Quantification was performed using StereoInvestigator Software "Optical Fractioner Workflow" probe with the following settings. Thickness of 50 μm was manually defined, and regions were selected using a 1.25x/0.03 (420310-9900) apochromat air objective for low magnification and then counted with a 10x/0.45 (420640-9900) apochromat air objective for high magnification. The border between medial septum (MS) and diagonal band of Broca (DB) was defined as a line between the two major island of Caleja. The regions were separated using different lines. The counting frame used was a square of 75-μm size and the grid was a square of 150-μm size. The counter was blind to genotype.

Oral administration of Donepezil

Donepezil hydrochloride (Sigma Aldrich, D6821) was orally administered in a jelly. Mice were trained to voluntarily consume jelly following the protocol described by Zhang (2011). Mice were given placebo jelly or a jelly containing a Donepezil dose of 1.8 mg/kg. For experiments studying the effects of Donepezil on acetylcholinesterase (AChE) activity, jelly was given at 8 A.M. daily. For experiments studying the effects of Donepezil on IIS, jelly was given daily at either 8 A.M., or 8 P.M. to assess interactions of AChE modulation and circadian cycle. Since there was no effect of AChE on IIS, results were pooled.

AChE assay

Quantitative measurements of AChE enzymatic activity were made using a modified Ellman method (Ellman et al., 1961; Rosenfeld et al., 2001). Stock solutions were acetylthiocholine iodide, used as the enzymatic substrate (ATH; 1.7 mg/ml in PBS, Sigma-Aldrich), 5,5'-dithio-bis(2-nitrobenzoic acid) (DTNB; 0.8 mg/ml in PBS, Sigma-Aldrich). Briefly, brains were rapidly dissected from either WT or J20 mice. Neocortex was isolated, weighed, and then homogenized using a Pellet Pestle (Sigma, Z 359971) in nine volumes of 0.1 M sodium phosphate buffer (pH 7.4; Patel et al., 2014). Five microliters of brain homogenate was aliquoted into each well of a 96-well plate, volume made up to 200 μl with PBS. DTNB (50 μl from stock) was added, followed by 50 μl of ATH substrate from stock. Measurement of absorption at 450 nm began immediately (<2 h from dissection) and was measured every 5 min for up to 30 min using a MRX microplate reader (Dynex Technologies). Thiocholine production in the test wells was expressed in units of nmol/min, calibrated with reference to the absorbance change over a range of concentrations giving a linear response using glutathione as the DTNB reactant (Eyer et al., 2003). Neostigmine (10 μM, Sigma-Aldrich) was used to completely inhibit AChE activity and establish that there was no baseline drift during the measurements.

Human scalp EEG and foramen ovale (FO) electrode recordings

Human scalp EEG and FO electrode recordings were performed at the Massachusetts General Hospital, as described in detail previously (Lam et al., 2017). Scalp EEG electrodes were placed using the International 10-20 system, with additional T1 and T2 electrodes.

Sleep staging in patient data were performed by a board-certified clinical neurophysiologist (ADL) based on visual analysis of the full scalp EEG data. While dedicated electro-oculogram and electromyogram channels were not recorded for these studies, the frontopolar scalp EEG electrodes allowed assessment of eye movements, while the frontopolar, frontal, and temporal electrodes allowed assessment of myogenic activity. Scalp EEG data were reviewed in 30-s epochs in the longitudinal anterior-posterior bipolar montage, using the Python module *wonambi* (https://github.com/wonambi-python/wonambi). Each 30-s epoch was classified as awake, non-REM (NREM)1, NREM2, NREM3, or REM, based on the American Academy for Sleep Medicine's manual for sleep scoring.

Spike quantification in patient data were performed by a board-certified clinical neurophysiologist (ADL), using a custom-made GUI in MATLAB (Mathworks). The GUI displayed 15-s epochs of left and right sided FO data, in both bipolar and common reference montages (common reference = C2), along with the EKG trace to allow exclusion of EKG artifact. The reviewer could adjust amplitudes for each trace as needed. For the MCI patient analyzed, contact #3 from the left FO electrode did not record properly and was excluded from analysis. The reviewer marked all spikes in each epoch. Epochs were presented in consecutive order, but the reviewer was otherwise blinded to the sleep stage for each epoch during the review. Instantaneous spike rates were calculated by determining the total number of left FO and right FO spikes detected within all 30-s epochs of the recording (which corresponded to the sleep staging epochs above) and converting these rates to spikes per hour. Average spike rates within each sleep stage were calculated by summing the total number of spikes that occurred during each sleep stage and dividing by the total number of hours the patient spent in each respective sleep stage in the recording.

Spectral analysis of the FO electrodes was performed in MATLAB, using the freely available Chronux toolbox (Mitra and Bokil, 2007). Analysis was performed on the LFO1, LFO2, RFO1, and RFO2 channels, as these were the deepest contacts and thus least prone to noise or artifact. Channels were each normalized to zero-mean, unit-variance. Multi-taper spectrograms were calculated for each normalized channel, using the Chronux script *mtspecgramc* with the following parameters: frequency range: 1–20 Hz, window: 30 s; step size: 30 s; time-bandwidth product: 3, tapers: 5. This provided a spectral resolution of 0.2 Hz. An average spectrogram across all FO channels was then generated, and the average spectral powers within the δ-band (0–4 Hz) and θ-band (4–12 Hz) were then calculated.

Statistics

Statistical data analysis was performed using R (version 3.2.0) including the "dplyr" (Wickham and Francois, 2015) and ggplot2 (Wickham, 2009) packages.

Assumptions for parametric tests were tested using Q-Q plots and residual plots. Data transformations or nonparametric tests were used for two-group comparisons in which test assumptions were violated.

For evaluating the effects of the fixed effects of age and genotype on the proportion of intervals containing more than one spike in APP$^{NL/F}$ animals, the data first underwent a square-root transformation and then fit using a linear model:

$$\sqrt{Interval\ Proportion} \sim Age + Genotype + \varepsilon$$

where ε is the error term.

The time of IIS was treated as circular variable. Each interval in which one or more IISs were detected was considered an event. The time of each event was evaluated as a phase of a circadian cycle. Circular data were analyzed using circular statistics by means of the "circular" package (Agostinelli and Lund, 2013). Circular outliers were identified using "CircOutlier" package (Rambli et al., 2016).

For tests entailing random variables, linear mixed models were fit using "lme4" (Bates et al., 2015). Significance was tested using a log-likelihood test comparing the full model to a null model without the factor of interest.

For evaluation of the relationship between spike count and θ/δ, we described each θ/δ value as a member of one of three levels: (1) $\theta/\delta \leq 1$; (2) $1 < \theta/\delta \leq 2$, and (3) $\theta/\delta > 2$. We then modeled spike count (Poisson-distributed) as a function of levels of θ/δ, using the R package "MCMCglmm" (Hadfield, 2010). It should be noted that due to poor properties of a single model fitted across all animals (fitting animal as a random effect and θ/δ factor as a fixed effect), separate models were fitted to individual animals without including a random effect. Thus, the data do not allow for inference about the population.

Event-triggered averages of IISs were evaluated by considering each interval in which an IIS was detected as an event. If no intervals within ± 80 s around the event were excluded, then the 160-s window was included in the calculation of the event-triggered averages, else the event was excluded from the averaging. An event-triggered average was also evaluated around 2000 randomly sampled points.

For comparing θ/δ in intervals with IIS to θ/δ in intervals preceding IIS, we considered only interval pairs where the preceding interval did not contain IIS and fit the model

$$(\theta/\delta)^{1/4} \sim Index + Subject + \varepsilon$$

where Index was a factor labeling whether the interval contained IIS or the preceding interval and modeled as a fixed effect, and Subject was a random effect with a random intercept.

For comparison of ChAT+ cells between genotypes, the model used was:

$$Estimated\ Count \sim Genotype + Region + Subject + \varepsilon$$

where Genotype and Region were fixed effects and Subject was a random effect with a random intercept.

To study the effect of genotype and treatment of the Thiocholine production rate, the data of Thiocholine production was log-transformed. The model used was

$$log\ (Thiocholine\ Rate) \sim Genotype\ Treatment + Repeat\ ID + \varepsilon$$

where GenotypeTreatment was a fixed effect and RepeatID was a random effect with a random intercept. *Post hoc* tests for the linear model were performed using package "multcomp" with the Holm correction method (Hothorn et al., 2008). It should be noted that while the treatment levels of control and donepezil were independent, the neostigmine treatment was applied to a sample of WT control tissue and thus was not independent. This repeated factor was not accounted for in the model.

Significance was tested using $\alpha = 0.05$. Two-sided hypothesis testing was used.

Superscripts following statistical reporting in the results section refer to the statistical table (Table 1).

Code and data accessibility

The processor script used for quantification of IIS, θ, and δ power in rodent ECoG data are available from http://www.opensourceinstruments.com/Electronics/A3018/HTML/SCPP4V1.tcl.

Code used for quantifying IIS in human data are available from https://github.com/mauriceaj/GUI-EEG_Spike_Annotation.

The datasets used for Figures 1–6 (rodent data) are available from http://dx.doi.org/10.7488/ds/2319.

Results

Network hyperexcitability in mouse models of AD pathology

To establish circadian patterns of network hyperexcitability in J20 mice, we recorded ECoG activity from freely-moving J20 and littermate WT mice using wireless telemetry over a period of 3 d. As network excitability has been suggested to be an early event in AD pathogenesis (Vossel et al., 2013; Sarkis et al., 2016), we focused our study on ages which precede overt plaque pathology in J20s (Mucke et al., 2000).

As previously reported (Palop et al., 2007), nonseizure, IIS (Fig. 1A) were detected in J20 ECoG (note that while ictal activity was not assessed, we refer to these as interictal events due to the similarity with IIS that have been reported in the literature) . We applied automated event detection (see Materials and Methods), on 8-s intervals of continuous ECoG. The percentage of intervals in which 1 or more spikes were detected was negligible in WTs (mean percentage: 0.8%, SD = 0.7%, $n = 8$). In contrast, the percentage of intervals with 1 or more spikes was greater in J20s (mean percentage: 11.6%, SD = 5.1%, $n = 18$; $t(23.98) = 10.6$, $p < 0.0001$, t test on square root transformed data with Welch correction; Fig. 1B,C)[a].

Table 1. Statistical table

	Data structure	Type of test	Confidence/Credible interval (CI) parameter	95% CI
a	Normal (square root transformed)	*t* test	Difference of means of square root data	(0.20, 0.30)
b	Normal (square root transformed)	Linear mixed model	β-Genotype	(−0.01, 0.03)
			β-Age	(−0.02, −0.002)
c	IIS count data (analyzed with log-link function)	MCMC generalized model	Difference between estimates of $\theta/\delta < 1$ vs $\theta/\delta > 2$; provided for animals JF221, JF220, JF218, J0460, and J0456, respectively	(1.619, 2.122) (0.261, 0.471) (0.254, 0.478) (1.166, 1.392) (2.128, 2.372)
d	Normal (fourth root transformed)	Linear mixed model	β–Index	(−0.004, 0.008)
e	Normal	Linear mixed model	β-Genotype	(−1015.7, 1029.0)
f	Non-normal	Wilcoxon-signed rank test	Difference of medians	(0.08, 0.65)
g	Normal (log transformed)	Tukey contrasts	J20_Ctrl - WT_Ctrl	(−0.24, 0.03)
			WT_DPZ - WT_Ctrl	(−0.15, 0.12)
			J20_DPZ - WT_Ctrl	(−0.08, 0.19)
			WT_NSTG - WT_Ctrl	(−1.50, −1.23)
			WT_DPZ - J20_Ctrl	(−0.04, 0.23)
			J20_DPZ - J20_Ctrl	(0.02, 0.29)
			WT_NSTG - J20_Ctrl	(−1.40, −1.13)
			J20_DPZ - WT_DPZ	(−0.07, 0.21)
			WT_NSTG - WT_DPZ	(−1.49, −1.22)
			WT_NSTG - J20_DPZ	(−1.56, −1.29)
h	Normal	Paired *t* test	Difference of mean IIS rate	(−0.01, 0.03)

Seizures and IIS have been reported in numerous strains of transgenic mice that express hAPP and that exhibit Aβ pathology (Del Vecchio et al., 2004; Palop et al., 2007; Minkeviciene et al., 2009; Rasch and Born, 2013). However, it has been suggested that such network hyperexcitability is the result of overexpression of hAPP (Born
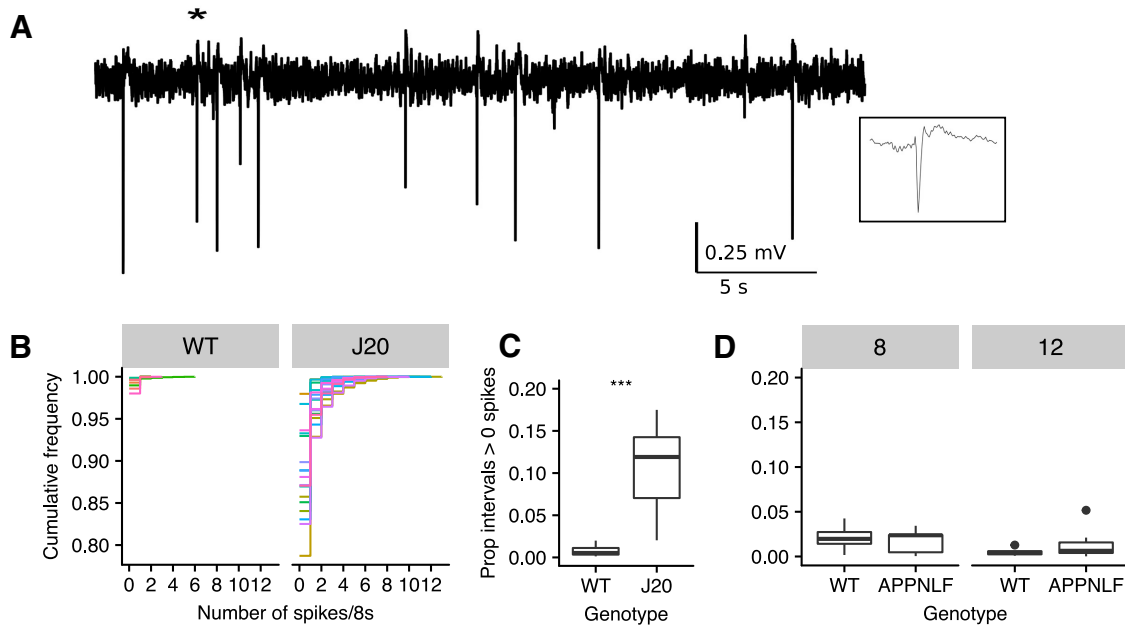
Figure 1. IISs are prevalent in J20 mice but not in APP knock-in mice. ***A***, ECoG trace recorded from a J20 mouse showing IIS. Inset is 250-ms expansion around IIS event marked by ∗. ***B***, Empirical cumulative distribution frequency plots for individual animals quantifying the number of detected IIS in 8-s intervals across 3 d of recording in WT and J20s. Colors represent distributions for individual animals. ***C***, Plot showing the proportion of intervals with one or more detected IIS in WT and J20. ***D***, Plot showing the proportion of intervals with one or more detected IIS in WT and APP[NL/F] at eight and 12 months. Bars represent medians. Whiskers extend to 1.5 interquartile range and data points outside of this range shown as points; ∗∗∗$p < 0.001$.

et al., 2014). To determine whether network hyperexcitability is associated with Aβ pathology in the absence of hAPP overexpression, we performed telemetric ECoG recordings as above, in mice expressing the humanized Aβ sequence of APP (APP[NL/F]; Saito et al., 2014) and age-matched controls. We recorded from mice at ages preceding overt plaque pathology (eight months) and at ages where plaques begin to appear (12 months; Saito et al., 2014; Masuda et al., 2016). We found no significant effect of genotype in the proportion of intervals containing spikes between WT and APP[NL/F] ($F_{(2,32)} = 3.1$, $R^2 = 0.11$, $p = 0.06$; Fig. 1D)[b] with a negligible proportion of intervals with one or more spikes detected [mean percentage of intervals with one or more spikes, pooled across genotype and age = 1.2%, 95%CI (0.8%, 1.6%)]. A *post hoc* power calculation based on the effect size from the J20 group (Cohen's $d = 2.5$) and the sample sizes of the APP[NL/F] and WT groups yielded a power of >0.99 at $\alpha = 0.05$ for an effect of genotype. Hence, we conclude that APP[NL/F] mice show no evidence of network hyperexcitability compared to control animals.

Circadian coupling of IIS

It has been suggested that seizure-related activity shows circadian fluctuations in epilepsies (Quigg, 2000). Hence, we next asked whether the likelihood of IIS in J20s varies across the day/night cycle. Quantifying the number of IIS per hour revealed that IIS are more frequent during daylight hours (inactive phase; Fig. 2A). We used circular statistics to extract measures of the phase coupling of IIS to the circadian cycle within individual J20 animals (see Materials and Methods). To evaluate the degree of phase coupling of IIS in each animal, we evaluated the mean angular vector length (ρ) from the time of IIS. ρ can vary between 0 (no phase coupling) and 1 (perfect phase coupling). To evaluate the time to which IISs were coupled, we extracted the mean coupling phase off IIS, expressed as a time on a 24-h cycle (φ_{IIS}).

The distribution of IIS phases differed significantly from a random distribution in all animals (Rayleigh test of uniformity: $p < 10^{-11}$). The extent of phase coupling was variable across the sample of J20s (mean $\rho_{IIS} = 0.24$, SD = 0.13, $n = 16$; Fig. 2B).

Evaluating the coupling phase revealed that IIS occurred predominantly in the light condition (Fig. 2A). Across the sample of J20s, the mean φ_{IIS} ($\overline{\varphi_{IIS}}$) confirmed this ($\overline{\varphi_{IIS}} = 15h05$, $\rho = 0.38$, $n = 16$, $p < 0.0001$, Rayleigh's test; Fig. 2B). Inspection of the φ_{IIS} distribution revealed potential outliers. Testing for outliers on a circular distribution (Rambli et al., 2016) identified four outliers. These four animals were among the five that showed a cluster of weakest phase coupling as measured by ρ_{IIS} (range: 0.06–0.11). We used the upper bound of the range of ρ_{IIS} of the four outlier animals to classify phase coupling as weak or strong. Henceforth, we refer to the five animals with $\rho_{IIS} \leq 0.11$ as showing weak phase coupling, and the other 11 animals as showing strong phase coupling ($\rho_{IIS} > 0.17$).

Sleep/wake modulation of IIS

Since IIS predominantly occurred in the normal inactive phase of the circadian cycle, we next asked whether this
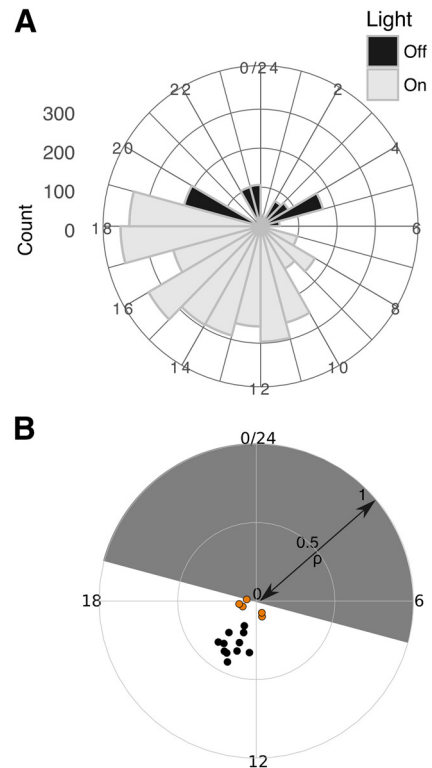
Figure 2. Circadian modulation of IIS. ***A***, Circular histogram of IIS counts over 3 d of recording in an individual J20 mouse plotted on 24-h cycle. Light condition indicated by shading. For the animal shown, $\varphi_{IIS} = 14$ h 51 min and $\rho = 0.35$. ***B***, Summary data for φ_{IIS} versus ρ for all animals, shown on circular plot. Solid symbols are strongly-coupled animals. Weakly coupled animals are shown with orange fill.

circadian modulation of IIS could be accounted for by the sleep/wake state of the animals. In a subset of J20s, we acquired simultaneous video recordings while recording ECoG data ($n = 4$). We manually scored the video and classified periods as sleep or wake (see Materials and Methods). Two of these four J20 animals showed strong circadian phase coupling of IIS, and two showed weak phase coupling. For the two animals that showed strong phase coupling of IIS, IIS occurred more frequently in sleep than during waking (Fig. 3A,B). In contrast, the modulation of IIS probability did not show a consistent pattern in animals showing weak phase coupling (Fig. 3B). This suggests that the strong phase coupling of IIS may be accounted for by differences in behavioral state across the circadian cycle.

Brain state modulation of IIS in J20 mice

Sleep-related ictal and interictal activity is differentially modulated by REM and NREM sleep in different forms of epilepsy (Bazil and Walczak, 1997; Herman et al., 2001; Sedigh-Sarvestani et al., 2014; Ewell et al., 2015). REM and NREM can be distinguished by the relative power in the δ (defined here as 0.1–3.9 Hz) and θ (4–12 Hz) frequency bands, with high θ/δ associated with REM (Ewell et al., 2015) as well as waking exploration (Buzsáki, 2002). Thus, we next asked whether IIS are more likely to occur
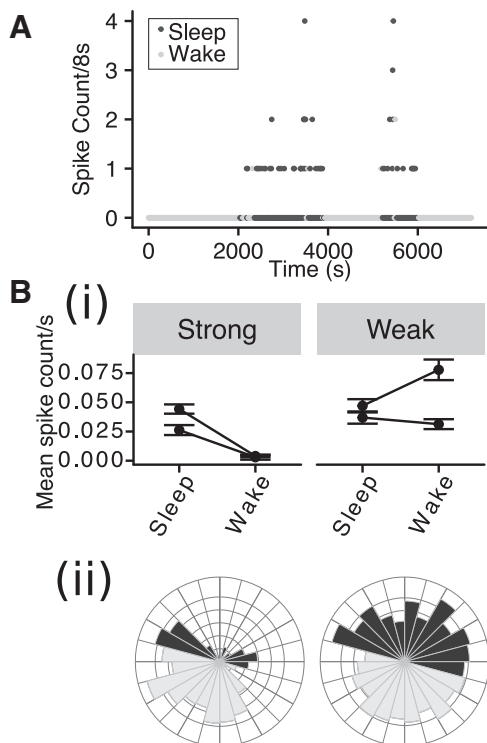
Figure 3. The probability of IIS is modulated by behavioral state in strongly phase-coupled animals. ***A***, IIS count/8-s interval versus time over 2 h of ECoG recording in a J20 mouse, with sleep and wake indicated by shading. ***Bi***, Mean spike rate in sleep and wake condition for strongly and weakly phase coupled animals. Error bars: 95% Confidence intervals (CI). ***Bii***, Circular histograms for a strongly (left) and weakly (right) phase coupled animals using conventions as in Figure 2*A*.

in particular brain states. To this end, we performed spectral analysis of the ECoG data from a subset of the mice (*n* = 5 J20s) in which a reference electrode was implanted at cerebellar coordinates (a noncortical reference for detection of cortical rhythms). ECoG recordings from J20 mice, exhibited periods showing a peak in θ-band power when animals were either awake (i.e., moving) or asleep, while periods of elevated δ-band power were seen during sleep (Fig. 4*A*). We evaluated the θ/δ ratio for each 8-s interval and related it to the number of IIS in the interval. Transient increases in θ/δ were observed during sleep and were associated with increased occurrences of IIS (Fig. 4*B*).

To quantify whether IIS were more likely in particular brain states, we next investigated the relationship between θ/δ and IIS count/8-s interval. As we were interested in discriminating between REM and NREM sleep, we limited the analysis to daylight hours when animals are more likely to be asleep. We used a value of θ/δ <1 and >2 to classify periods as NREM-like and REM-like, respectively (Ewell et al., 2015). This revealed significantly higher spike counts during REM-like versus NREM-like periods in all five animals (*p* < 0.0005 for all five animals, Markov Chain Monte Carlo generalized linear model; Fig. 4*B*)[c]. Interestingly, IISs were associated with increased θ/δ in animals showing both weak and strong phase coupling (Fig. 4*C*). Since sleep and wake are not predic-

tive of IIS in animals with weak phase coupling, this suggests that there is a mismatch between θ/δ and behavioral state in animals with weak phase coupling. Moreover, high θ/δ states are predictive of IIS, regardless of behavioral state.

To examine the temporal dynamics of θ/δ around IIS, we evaluated the IIS-triggered average of θ/δ (Sedigh-Sarvestani et al., 2014) for 160-s window around each interval in which at least one IIS was identified. In all animals, θ/δ was increased around the time of IIS relative to θ/δ averaged around randomly sampled points (Fig. 4*D*). In three strongly phase-coupled animals, θ/δ returned to baseline levels within the 160-s window around the event. However, in the weakly phase coupled animals, θ/δ remained elevated above baseline levels in this window. The peak in the θ/δ IIS-triggered average did not occur at $t = 0$ in any of the animals. Since intervals neighbouring the IIS-containing interval show increased θ/δ, this suggests that the IIS contribution to spectral power did not underlie the association between increases in θ/δ and IIS probability. To further examine whether IIS could directly contribute to the increased θ/δ, we compared θ/δ in intervals with IIS to θ/δ in the preceding intervals only in cases where the preceding interval contained no IIS. We found no significant difference in θ/δ between intervals with IIS and the preceding interval (linear mixed model, $\chi^2(1) = 0.35$, $p = 0.56$; data not shown)[d].

To determine whether the spectral ECoG patterns in J20 mice are a reflection of normal sleep or a result of pathology, we performed similar analysis of video-scored ECoG data from three WT mice. As in the J20, intervals of strong θ power were evident during wake and sleep, while periods of prominent δ-band activity were seen in sleep. Transient increases in θ/δ during sleep akin to those seen in J20s were also observed in all WT animals, suggesting that such increases are a feature of normal sleep, and not pathologic (Fig. 5). To compare the distribution of θ/δ during sleep between genotypes, we calculated the range and 90th percentile of θ/δ while animals were asleep (using data for which we had video scoring). Group sizes were too small for statistical comparison but suggested that θ/δ values spanned a narrower range in J20 mice than in WT mice [J20 mean range = (0.02, 10.0), 90th percentile = 2.4, SD(1.1), *n* = 4; WT mean range = (0.04, 19.3), 90th percentile = 5.4, SD(1.4), *n* = 3; data not shown].

No evidence of cholinergic changes in J20 mice

Cholinergic levels exhibit a circadian modulation (Hut and Van der Zee, 2011), and high cholinergic tone is implicated in generating θ oscillatory states (Buzsáki, 2002). In addition, cholinergic dysfunction has been suggested to be a key feature of AD pathogenesis (Craig et al., 2011). Recently, it has been suggested that cholinergic alterations may contribute to network excitability in the Tg2576 model of AD (Kam et al., 2016). Hence, we hypothesized that cholinergic changes might underlie the brain-state dependent modulation of IIS in the J20 mice. We used immunohistochemistry to quantify the number of ChAT+ cells in the MS and DB and asked whether the number of ChAT+ cells differs between J20 (*n* = 7) and
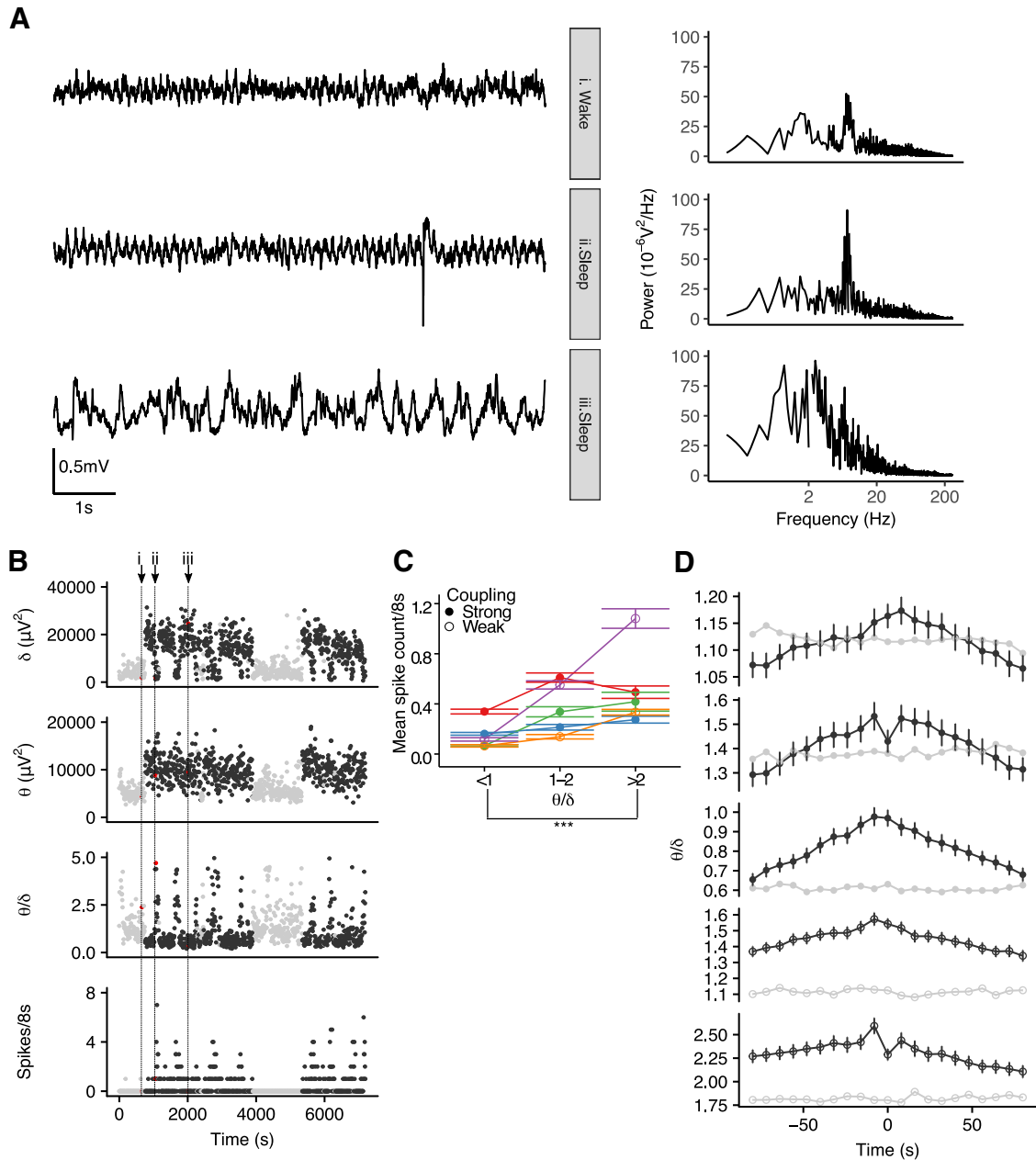
Figure 4. IIS occur during high θ/δ states. **A**, 8-s ECoG signals (left) and corresponding power spectra (right) during different behavioral states recorded from a J20 mouse. A single IIS is seen in the sleep high θ state (ii). **B**, Time series of δ power, θ power, θ/δ, and spike count per 8-s intervals across 2 h of ECoG recorded from the same J20 mouse as shown in **A**. Black/gray symbols indicate sleep/wake as classified by simultaneous video data. Red symbols and vertical dotted lines indicate the 8-s intervals for which the ECoG signal is shown in **A**. **C**, Spike number per 8-s interval as a function of θ/δ in five animals (represented by different colors and connected by lines). The increase spike count in intervals with high θ/δ was seen in animals with both strong (filled symbols) and weak (open symbols) circadian phase coupling; ***$p < 0.001$. **D**, IIS-triggered averages of θ/δ for five individual animals (black) and windowed averages triggered around 2000 randomly sampled points (gray) show an increased θ/δ around IIS. Strong/weak coupling shown in filled/open symbols. Error bars in **B**, **C** represent 95% CI.

WT ($n = 5$) mice. Fitting a linear mixed model to the data, we found no effect of genotype on the estimated number of ChAT+ cells in the MS or DB (linear mixed model, $\chi^2(1) = 0.0002$, $p = 0.99$; Fig. 6A)[e].

AChE activity is reduced in AD (García-Ayllón et al., 2011). We assayed cholinergic function by measuring AChE activity. AChE activity was quantified by estimating the rate of thiocholine production in neocortical brain homogenates (see Materials and Methods). There was no significant difference in the rate of thiocholine production in brain homogenates prepared from WT and J20 mice ($V = 15$, $p = 0.06$, $n = 5$ WT/J20, Wilcoxon signed rank test, matched by day of assay; Fig. 6B)[f]. We also wanted to directly test the effect of modulation of ACh levels on IIS. However, using oral administration of Donepezil at a dose previously suggested to achieve clinically relevant
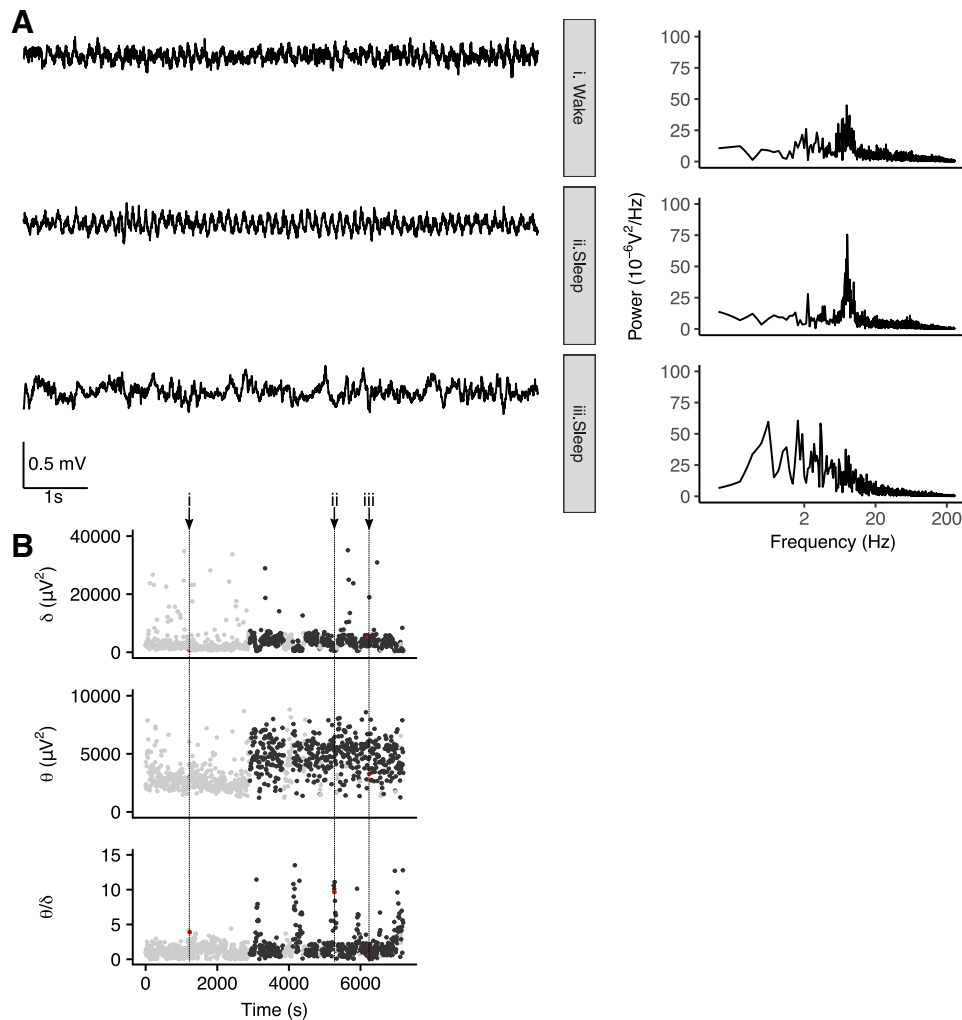
Figure 5. Transient increases in θ/δ are nonpathologic features of sleep. ***A***, 8-s ECoG signals (left) and corresponding power spectra (right) during different behavioral states recorded from a WT mouse. ***B***, Time series of δ power, θ power, and θ/δ per 8-s interval across 2 h of ECoG recorded from same WT mouse as shown in ***A***. Black/gray symbols indicate sleep/wake as classified by simultaneous video data. Red symbols and vertical dotted lines indicate the 8-s intervals for which the ECoG signal is shown in ***A***.

drug plasma levels (Dong et al., 2009) was ineffective at altering AChE activity in brain homogenates. In contrast, a positive control treatment of direct application of neostigmine to brain homogenate led to a significant reduction in AChE activity (linear mixed model: $\chi^2(4) = 73.5$, $p < 0.0001$; *post hoc* using Tukey paired comparisons: $p < 0.0001$ for neostigmine versus each of the treatment and genotypes; $p > 0.05$ for all other group comparisons; Fig. 6B)[g]. Two days of oral Donepezil administration at this dose did not affect the IIS rate in J20 mice ($t_{(11)} = 0.8$, $p = 0.43$, paired t test; data not shown)[h].

Sleep stage modulation of IIS in human AD

The first intracranial recordings in humans with AD were recently reported and demonstrated marked activation of mesial temporal lobe (mTL) IIS during sleep compared to the awake state (Lam et al., 2017). We further analyzed the combined scalp EEG and intracranial electrode recordings from these two patients to better understand the relationship between sleep stage and mTL IIS rate in AD patients. One patient with advanced AD did not achieve REM sleep but showed mTL IIS preferentially during NREM sleep as opposed to waking states (Table 2, patient 1). The second patient was a 67-year-old woman with amnestic MCI (aMCI), an early stage of AD that is thought to correspond to the early stage of AD modeled in our young J20 mice. The data from this patient were used to compare the frequency of IIS in wake, NREM, and REM states.

We analyzed 14.25 consecutive hours of combined scalp EEG and FO recordings from the aMCI patient, which spanned from ~7 P.M. on the first day of FO recording (FOD1) to 9:15 A.M. the following morning (FOD2). Further recordings were not analyzed, as the patient was initiated on treatment with the anticonvulsant levetiracetam on the afternoon on FOD2. Of note, the patient underwent implantation with FO electrodes on FOD1 from ~12:40 to 1:50 P.M. and received sevoflurane, Propofol, and midazolam during the procedure. She was awake and answering questions appropriately by 2:15 P.M. on FOD1.
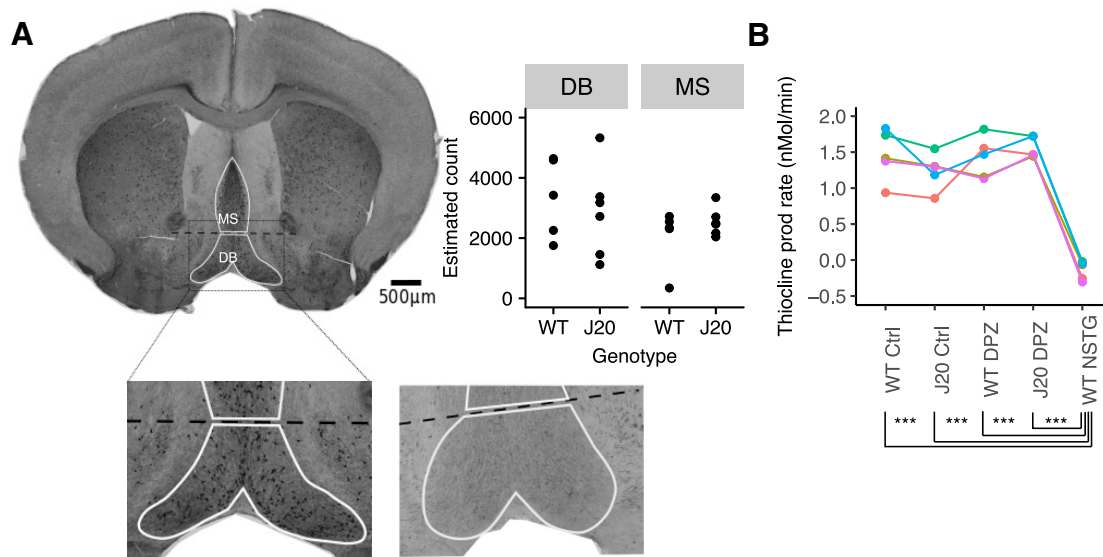
Figure 6. No evidence of cholinergic alterations in J20s. **A**, Immunostained brain section showing ChAT+ cells in MS and DB. Lower panel shows zoomed in region of upper panel (left) and corresponding regions of a negative control stained section (right). Upper right: Quantification of stereological estimates of ChAT+ cell count in MS and DB in WT and J20. Points represent estimated counts in individual animals. **B**, AChE activity was assayed by the rate of thiocholine production in brain homogenate from WT and J20 in control conditions and following oral administration of Donepezil (DPZ). The AChE activity was compared to a positive control of direct application of neostigmine (10 μM) to the brain homogenate. Experimental repeat groups are indicated by different colors and connected lines; ∗∗∗$p < 0.001$.

We performed sleep staging of the recording using the full scalp EEG data and measured mTL spike rates using the bilateral FO electrode data (Fig. 7A,B). As described previously, we found that mTL spiking in the aMCI patient was largely activated during sleep. In contrast to what we found in the young J20 mice, mTL spiking in the aMCI patient occurred with highest frequency during NREM sleep stages, particularly during NREM3, and were lowest during REM sleep (Fig. 7; Table 2). mTL IIS rates during REM sleep were also markedly lower than during wakefulness (Table 2). We also calculated spectral power in the θ- and δ-bands, as well as the θ/δ ratio, in the FO electrodes across sleep states (Fig. 7C–E). Increases in both θ and δ power were seen with deepening stages of NREM sleep, while a reduction was seen with REM sleep. In contrast to what we observed in the J20 mice, the θ/δ ratio

was reduced during periods of highest spike frequency (Fig. 7E).

Discussion

Network hyperexcitability is a feature of AD. Here, we compared patterns of network hyperexcitability in two rodent models of AD, as well as in two AD patients, to reveal shared phenomenological features with the disease. We show that while J20 (hAPP overexpressing) mice exhibit frequent IIS as previously reported, APP[NL/F] mice (which express APP at physiologic levels) do not show evidence of network hyperexcitability. Moreover, IIS in J20s occur primarily during daylight hours, and this circadian fluctuation is accounted for by an increased probability of IIS during sleep. Interestingly, we found that IIS in J20 mice are modulated by brain state, with increased likelihood of IIS in brain states with high θ/δ activity, a marker of REM sleep. In contrast, patients with AD showed prevalent IIS during NREM sleep. Moreover, in the one AD patient who exhibited REM sleep, IIS frequency was lowest in REM compared to other states.

Circadian dysfunction and network hyperexcitability in AD

Brain network hyperexcitability in the form of IIS and seizures has now been reported in numerous models of AD pathology (for review, see Scharfman, 2012; Born, 2015). Our data, along with those reported by others (Born et al., 2014; Kam et al., 2016) reveal that network hyperexcitability in animals models of AD can be modulated by the circadian cycle. Circadian disturbances in AD include sleep fragmentation, increased daytime somnolence, and

Table 2. Average mTL spike rates were evaluated from FO electrodes and related to sleep stage as assayed by scalp EEG in two patients with AD

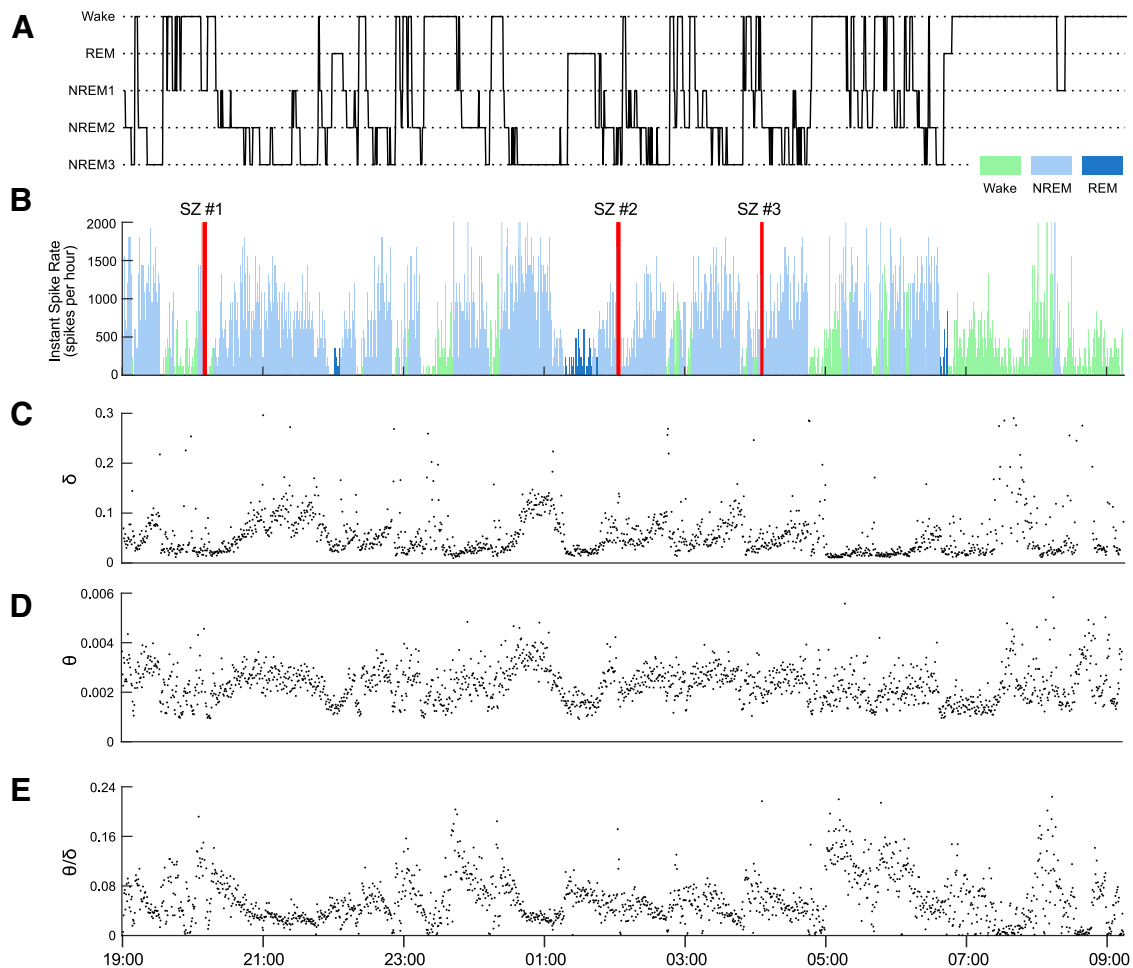| Sleep stage	Patient 1 (AD dementia)		Patient 2 (aMCI)	
	Total hours in record	Average spike rate (spikes/hour)	Total hours in record	Average spike rate (spikes/hour)
Wake	4.7	11	5.2	329
NREM1	0.7	31	1.5	670
NREM2	2.1	80	3.8	739
NREM3	1.4	62	3.1	903
REM	0	n/a	0.7	159

Figure 7. Sleep stage coupling of mTL spiking in a human with aMCI, a suspected early stage of AD. **A**, Hypnogram showing the patient's sleep architecture, spanning from ~7 P.M. on FOD1 to 9:15 A.M. on FOD2. **B**, Bar plot showing instantaneous mTL lobe spike rates over the course of the recording. Bars are colored by sleep stage, with light green for Wake, light blue for NREM (includes NREM1, NREM2, and NREM3), and dark blue for REM. The patient had three brief subclinical seizures (SZ) from the left FO electrodes during this recording, the timing of which is depicted by red vertical bars. **C–E**, Plots showing (**C**) δ power (0–4 Hz), (**D**) θ power (4–12 Hz), and (**E**) θ/δ ratio of bilateral mTL activity, based on FO electrodes recordings. Dots represent the spectral power for each nonoverlapping 30-s window of the recording. Power is measured in arbitrary units.

sundowning, the phenomenon in which neuropsychiatric symptoms are heightened late in the day (Peter-Derex et al., 2015). Animal models of AD have also been reported to show disturbances in the circadian cycle, some of which overlap with patterns of circadian alterations seen in patients (Huitrón-Reséndiz et al., 2002; Vloeberghs et al., 2004; Wisor et al., 2005; Jyoti et al., 2010; Sterniczuk et al., 2010; Duncan et al., 2012; Roh et al., 2012). Our findings of circadian modulation of network hyperexcitability in AD raise the question of whether IIS might causally contribute to the alterations in circadian-coupled behavior observed in AD. Future work investigating the effects of anti-epileptic drugs on circadian alterations in AD would go toward answering this.

Brain state modulation of network excitability

Here, we report that IIS in J20 animals are modulated by θ/δ, with higher IIS rates seen in states of high θ/δ during sleep. The spectral patterns of ECoG that we report here are in line with previous reports in WT mice,

that have shown increases in cortical EEG θ power in REM sleep relative to wake and NREM (Brankack et al., 2010). We also report transient increases in θ/δ in sleep in both WT and J20 mice. Since these increases in θ/δ occur in both WT and J20s, they are likely to be indicative of REM sleep periods (Ewell et al., 2015). Given that J20 animals with strong circadian phase coupling show highest IIS rates during sleep this suggests that IIS in these animals are associated with REM sleep.

An alternative explanation for the association between IIS and high θ/δ during sleep may be that IIS occur during ectopic θ in sleep, in the absence of a concomitant drop in muscle tone. A phenomenon of ictal activity during ectopic θ has been reported in a mouse model of Huntington's disease (Pignatelli et al., 2012). Without simultaneous EMG recordings, the present data cannot conclusively distinguish between REM states and ectopic θ. In the human data, analysis of θ/δ ratios showed that these were lowest during periods of highest IIS frequency. This argues against the idea of IIS coupled to ectopic θ in humans,

although a more definitive assessment will require data from more AD subjects as well as healthy elderly controls.

Our finding of an association between IIS and high θ/δ is in line with recent reports that young Tg2576 model of AD as well as mice overexpressing WT-hAPP also demonstrate IIS predominantly during states of high θ which the authors suggest is indicative of REM sleep (Kam et al., 2016).

The findings that IIS in multiple mouse models of AD are most likely to occur in REM-like states begs the question of what makes REM a proictal state in these models. Both REM sleep and the awake state share common features of high θ/δ activity and high cholinergic tone (Vazquez and Baghdoyan, 2001; Lee et al., 2005), yet IIS occur much less frequently in the awake state in these models. There are several potential explanations for this. Firing rates of hippocampal neurons increase during REM (Grosmark et al., 2012), which might contribute to the propensity to seize. In addition, systems that normally show distinct activity in REM sleep versus waking and NREM sleep might contribute to the proictal REM state in these models (Sedigh-Sarvestani et al., 2014; Ewell et al., 2015; Kam et al., 2016). Unlike cholinergic neurons, which increase their activity in both REM and waking, monoaminergic neurons in brainstem nuclei (including the locus coeruleus and the tuberomammillary nucleus) as well as the dorsal raphe nucleus of the hypothalamus, show differential activity between these brain states. These neurons are highly active in waking, exhibit low firing rates in NREM sleep, and are quiescent during REM sleep (Lee and Dan, 2012). It may be that brain state modulation of one or more of these systems is disrupted in these mouse AD models, and other forms of epilepsy which show REM coupling (Sedigh-Sarvestani et al., 2014; Ewell et al., 2015).

The present study quantified cholinergic neurons in MS and DB. Cholinergic neurons in laterodorsal tegmental and pedunculopontine tegmental nuclei of the pontomesencephalic tegmentum have been suggested to control REM onset (Van Dort et al., 2015). In the rat, these neurons have been shown to be active during both wake and REM; however, firing rates are higher in REM, and correlate with θ/δ (Boucetta et al., 2014). Thus, changes to these neurons are also potential candidates for mediating the proictal nature of REM sleep in J20 mice.

Kam et al. (2016) reported that MS-DB cholinergic neuron number was unchanged in young Tg2576 mice. However, they found evidence to support the notion that overactivity of cholinergic neurons might contribute to IIS by showing that antagonism of muscarinic receptors reduced IIS in these animals. Hence, they concluded that IIS during REM might be the result of cholinergic hyperfunction. We did not find evidence for cholinergic changes in J20 mice as quantified by the number of cholinergic neurons in MS-DB, or AChE activity. If cholinergic activity is indeed unaltered in J20 mice, future experiments using muscarinic antagonism in J20 mice could be used to investigate whether atropine can act to reduce IIS by reducing overall neuronal excitability, rather than by reversing cholinergic hyperfunction.

Our assay of cholinergic function was based on measurements of AChE enzymatic activity in brain homogenate. There was no significant difference between AChE levels in WT and J20, or with Donepezil treatment. While it is possible that postmortem degradation of AChE could have masked differences in AChE levels, the robust effect of neostigmine supports the conclusion that the tissue contained functional AChEs.

In a subset of our animals, IIS were weakly coupled to the circadian cycle and the sleep-wake pattern but were still modulated by θ/δ. This suggests that the relationship between θ/δ and behavioral state might be disturbed in these animals. It is possible that these animals also exhibited greater disturbances in other elements of the circadian cycle, such as a circadian decoupling of sleep quantity/quality.

During both REM and NREM, hippocampal neurons have been shown to replay firing patterns that were experienced before sleep (Skaggs and McNaughton, 1996; Louie and Wilson, 2001), and such precisely timed sequences are likely to be involved in the memory facilitation role of sleep. IIS are thought to arise from depolarization and synchronous firing of neurons. This firing is followed by an inhibition and reduction of firing (Holmes and Lenck-Santini, 2006). Thus, IIS during sleep are likely to interfere with the coordinated replay of firing sequences, and consequently, would be expected to contribute to memory impairments. In support of this, it has recently been shown that reducing IIS by treatment with antiepileptic drugs, rescues memory deficits in J20s (Sanchez et al., 2012).

Relationship between IIS and AD pathology in mouse models

Here we report that while IIS are prevalent in hAPP overexpressing mice, APP$^{NL/F}$ mice that exhibit Aβ pathology without APP overexpression, do not exhibit IIS at two ages preceding widespread plaque deposition (eight and 12 months). This finding is in line with other reports that it is overexpression of hAPP that is causal in generating network hyperexcitability in these animal models (Born et al., 2014; Xu et al., 2015; Kam et al., 2016). An alternative explanation of the presence of IIS in J20 but not APP$^{NL/F}$ mice may be differences in the levels of Aβ between the two models. However, levels of soluble Aβ in six-month-old J20 and 12-month-old APP$^{NL/F}$ are comparable, and levels of total Aβ are higher in APP$^{NL/F}$ (Shankar et al., 2009; Saito et al., 2014). Thus, it is unlikely that higher levels of Aβ in the J20s are a cause of IIS in this model.

Interestingly, APP$^{NL/F}$ mice begin to exhibit cognitive deficits at eight months of age (Masuda et al., 2016), which suggests that cognitive deficits at these ages are not the result of IIS, as has been suggested for J20s (Sanchez et al., 2012). Moreover, differences in the types of memory affected in J20 and APP$^{NL/F}$ at ages preceding overt plaque deposition have been reported. Specifically, four- to six-month-old J20s show impairments in hip-

pocampal dependent spatial memory (Sanchez et al., 2012). In contrast, in eight-month-old APP$^{NL/F}$ mice, spatial memory as assayed by a place preference task is intact. However, place-avoidance memory, which is also dependent on amygdala circuits (Wilensky et al., 2000), is impaired (Masuda et al., 2016). It may be that hippocampus dependent processes are susceptible to interference by IIS while the disturbances in the nonhippocampal circuits result from processes independent of IIS.

Differential sleep-stage coupling between mouse models of AD and human AD

Lam et al. (2017) recently used intracranial electrode recordings to detect mTL IIS in two AD patients without a history of epilepsy. Here, we report that in these patients, IISs were predominantly associated with NREM sleep (i.e., low θ/δ). In the patient with aMCI, IIS occurred most frequently in NREM3 sleep and were least frequent in REM, with a >4.5-fold difference in spike rates between NREM3 and REM. In the AD patient, frequent IIS were seen during NREM sleep, although REM sleep was absent from this patient's brief recording, in line with previous reports of REM deficits in AD (Vitiello et al., 1984). Our findings from intracranial electrodes in AD patients are consistent with prior scalp EEG studies by Vossel et al. (2016), who reported that epileptiform discharges are highly prevalent in sleep stages >2 (although the authors did not differentiate between REM and NREM sleep). Although the means of characterising sleep differed between rodents and patients, combined, these results point to important differences in sleep stage coupling of epileptiform activity between rodent AD models and humans with AD and suggest that the specific mechanisms that underlie hyperexcitability in AD may differ between certain mouse models and humans.

Analysis of ictal and interictal activity in epilepsy patients has led the view that NREM sleep is a generally proictal state, whereas REM sleep is an anti-ictal state (Sammaritano et al., 1991; Herman et al., 2001; Minecan et al., 2002; Ng and Pavlova, 2013). Many animal models of epilepsy have also shown that seizures are more frequent in NREM and rarely occur in REM (Shouse et al., 2000). Interestingly, rodent models of the same type of epilepsy can still exhibit differences in the sleep-stage coupling of epileptiform activity. For example, in both the kindling as well as the pilocarpine models of temporal lobe epilepsy in rats, IIS are most common during NREM sleep (Colom et al., 2006; Gelinas et al., 2016). In contrast, rats with either the tetanus toxin or the low-dose kainate models of temporal lobe epilepsy have seizures that occur most commonly during REM sleep (Sedigh-Sarvestani et al., 2014; Ewell et al., 2015). Based on this, we hypothesize that different mouse models of AD may have specific mechanisms underlying their network hyperexcitability, which could be differentially expressed through sleep-stage coupling of IIS. We propose that sleep-stage coupling of IIS should be an important factor for identifying mouse AD models that more closely resemble the EEG signature of network hyperexcitability in human AD.

References

Agostinelli C, Lund U (2013) R package "circular": circular statistics. Available at https://r-forge.r-project.org/projects/circular.

Amatniek JC, Hauser WA, DelCastillo-Castaneda C, Jacobs DM, Marder K, Bell K, Albert M, Brandt J, Stern Y (2006) Incidence and predictors of seizures in patients with Alzheimer's disease. Epilepsia 47:867–872. CrossRef Medline

Bakker A, Krauss GL, Albert MS, Speck CL, Jones LR, Stark CE, Yassa MA, Bassett SS, Shelton AL, Gallagher M (2012) Reduction of hippocampal hyperactivity improves cognition in amnestic mild cognitive impairment. Neuron 74:467–474. CrossRef Medline

Bates D, Mächler M, Bolker B, Walker S (2015) Fitting linear mixed-effects models using lme4. J Stat Softw 67:1–48. CrossRef

Bazil CW, Walczak TS (1997) Effects of sleep and sleep stage on epileptic and nonepileptic seizures. Epilepsia 38:56–62. Medline

Bero AW, Yan P, Roh JH, Cirrito JR, Stewart FR, Raichle ME, Lee J-M, Holtzman DM (2011) Neuronal activity regulates the regional vulnerability to amyloid-β deposition. Nat Neurosci 14:750–756. CrossRef

Bezzina C, Verret L, Juan C, Remaud J, Halley H, Rampon C, Dahan L (2015) Early onset of hypersynchronous network activity and expression of a marker of chronic seizures in the Tg2576 mouse model of Alzheimer's disease. PLoS One 10:e0119910. CrossRef Medline

Bookheimer SY, Strojwas MH, Cohen MS, Saunders AM, Pericak-Vance MA, Mazziotta JC, Small GW (2000) Patterns of brain activation in people at risk for Alzheimer's disease. N Engl J Med 343:450–456. CrossRef Medline

Born HA (2015) Seizures in Alzheimer's disease. Neuroscience 286:251–263. CrossRef Medline

Born HA, Kim J-Y, Savjani RR, Das P, Dabaghian YA, Guo Q, Yoo JW, Schuler DR, Cirrito JR, Zheng H, Golde TE, Noebels JL, Jankowsky JL (2014) Genetic suppression of transgenic APP rescues hypersynchronous network activity in a mouse model of Alzeimer's disease. J Neurosci 34:3826–3840. CrossRef

Boucetta S, Cissé Y, Mainville L, Morales M, Jones BE (2014) Discharge profiles across the sleep–waking cycle of identified cholinergic, GABAergic, and glutamatergic neurons in the pontomesencephalic tegmentum of the rat. J Neurosci 34:4708–4727. CrossRef Medline

Brankack J, Kukushka VI, Vyssotski AL, Draguhn A (2010) EEG gamma frequency and sleep–wake scoring in mice: comparing two types of supervised classifiers. Brain Res 1322:59–71. CrossRef Medline

Busche MA, Konnerth A (2015) Neuronal hyperactivity–A key defect in Alzheimer's disease? Bioessays 37:624–632. CrossRef Medline

Busche MA, Chen X, Henning HA, Reichwald J, Staufenbiel M, Sakmann B, Konnerth A (2012) Critical role of soluble amyloid-B for early hippocampal hyperactivity in a mouse model of Alzheimer's disease. Proc Natl Acad Sci USA 109:8740–8745.

Buzsáki G (2002) Theta oscillations in the hippocampus. Neuron 33:325–340. Medline

Chang P, Hashemi KS, Walker MC (2011) A novel telemetry system for recording EEG in small animals. J Neurosci Methods 201:106–115. CrossRef Medline

Cirrito JR, Yamada KA, Finn MB, Sloviter RS, Bales KR, May PC, Schoepp DD, Paul SM, Mennerick S, Holtzman DM (2005) Synaptic activity regulates interstitial fluid amyloid-beta levels *in vivo*. Neuron 48:913–922. CrossRef Medline

Colom LV, García-Hernández A, Castañeda MT, Perez-Cordova MG, Garrido-Sanabria ER (2006) Septo-hippocampal networks in chronically epileptic rats: potential antiepileptic effects of theta rhythm generation. J Neurophysiol 95:3645–3653. CrossRef Medline

Craig LA, Hong NS, McDonald RJ (2011) Revisiting the cholinergic hypothesis in the development of Alzheimer's disease. Neurosci Biobehav Rev 35:1397–1409. CrossRef Medline

Cretin B, Sellal F, Philippi N, Bousiges O, Di Bitonto L, Martin-Hunyadi C, Blanc F (2016) Epileptic prodromal Alzheimer's dis-

ease, a retrospective study of 13 new cases: expanding the spectrum of Alzheimer's disease to an epileptic variant? J Alzheimers Dis 52:1125–1133. CrossRef

Del Vecchio RA, Gold LH, Novick SJ, Wong G, Hyde LA (2004) Increased seizure threshold and severity in young transgenic CRND8 mice. Neurosci Lett 367:164–167. CrossRef Medline

Dickerson BC, Salat DH, Greve DN, Chua EF, Rand-Giovannetti E, Rentz DM, Bertram L, Mullin K, Tanzi RE, Blacker D, Albert MS, Sperling RA (2005) Increased hippocampal activation in mild cognitive impairment compared to normal aging and AD. Neurology 65:404–411. CrossRef

Dong H, Yuede CM, Coughlan CA, Murphy KM, Csernansky JG (2009) Effects of Donepezil on amyloid-β and synapse density in the Tg2576 mouse model of Alzheimer's disease. Brain Res 1303:169–178. CrossRef

Duncan MJ, Smith JT, Franklin KM, Beckett TL, Murphy MP, St Clair DK, Donohue KD, Striz M, O'Hara BF (2012) Effects of aging and genotype on circadian rhythms, sleep, and clock gene expression in APPxPS1 knock-in mice, a model for Alzheimer's disease. Exp Neurol 236:249–258. CrossRef

Ellman GL, Courtney KD, Andres V, Feather-stone RM (1961) A new and rapid colorimetric determination of acetylcholinesterase activity. Biochem Pharmacol 7:88–95. Medline

Ewell LA, Liang L, Armstrong C, Soltész I, Leutgeb S, Leutgeb JK (2015) Brain state is a major factor in preseizure hippocampal network activity and influences success of seizure intervention. J Neurosci 35:15635–15648. CrossRef Medline

Eyer P, Worek F, Kiderlen D, Sinko G, Stuglin A, Simeon-Rudolf V, Reiner E (2003) Molar absorption coefficients for the reduced Ellman reagent: reassessment. Anal Biochem 312:224–227. Medline

Filippini N, MacIntosh BJ, Hough MG, Goodwin GM, Frisoni GB, Smith SM, Matthews PM, Beckmann CF, Mackay CE (2009) Distinct patterns of brain activity in young carriers of the APOE-ϵ4 allele. Proc Natl Acad Sci USA 106:7209–7214. CrossRef Medline

García-Ayllón M-S, Small DH, Avila J, Sáez-Valero J (2011) Revisiting the role of acetylcholinesterase in Alzheimer's disease: cross-talk with P-tau and β-amyloid. Front Mol Neurosci 4:22 CrossRef

Gelinas J, Khodagholy D, Thesen T, Devinsky O, Buzsáki G (2016) Interictal epileptiform discharges induce hippocampal-cortical coupling in temporal lobe epilepsy. Nat Med 22:641–648. CrossRef Medline

Grosmark AD, Mizuseki K, Pastalkova E, Diba K, Buzsáki G (2012) REM sleep reorganizes hippocampal excitability. Neuron 75:1001–1007. CrossRef Medline

Haberman RP, Branch A, Gallagher M (2017) Targeting neural hyperactivity as a treatment to stem progression of late-onset Alzheimer's disease. Neurotherapeutics 14:662–676. CrossRef

Hadfield JD (2010) MCMC methods for multi-response generalized linear mixed models: the MCMCglmm. R package. J Stat Softw 33. CrossRef

Herman ST, Walczak TS, Bazil CW (2001) Distribution of partial seizures during the sleep–wake cycle: differences by seizure onset site. Neurology 56:1453–1459. Medline

Hesdorffer DC, Hauser WA, Annegers JF, Kokmen E, Rocca WA (1996) Dementia and adult-onset unprovoked seizures. Neurology 46:727–730. Medline

Holmes GL, Lenck-Santini P-P (2006) Role of interictal epileptiform abnormalities in cognitive impairment. Epilepsy Behav 8:504–515. CrossRef Medline

Horváth A, Sz´ucs A, Barcs G, Kamondi A (2017) Sleep EEG detects epileptiform activity in Alzheimer's disease with high sensitivity. J Alzheimers Dis 56:1175–1183. CrossRef

Hothorn T, Bretz F, Westfall P (2008) Simultaneous inference in general parametric models. Biom J 50:346–363. CrossRef Medline

Huitrón-Reséndiz S, Sánchez-Alavez M, Gallegos R, Berg G, Crawford E, Giacchino JL, Games D, Henriksen SJ, Criado JR (2002) Age-independent and age-related deficits in visuospatial learning, sleep–wake states, thermoregulation and motor activity in PDAPP mice. Brain Res 928:126–137. Medline

Hut RA, Van der Zee EA (2011) The cholinergic system, circadian rhythmicity, and time memory. Behav Brain Res 221:466–480. CrossRef Medline

Jyoti A, Plano A, Riedel G, Platt B (2010) EEG, activity, and sleep architecture in a transgenic AβPPswe/PSEN1A246E Alzheimer's disease mouse. J Alzheimers Dis 22:873–887. CrossRef Medline

Kam K, Duffy ÁM, Moretto J, LaFrancois JJ, Scharfman HE (2016) Interictal spikes during sleep are an early defect in the Tg2576 mouse model of β-amyloid neuropathology. Sci Rep 6:20119. CrossRef Medline

Kazim SF, Chuang S-C, Zhao W, Wong RKS, Bianchi R, Iqbal K (2017) Early-onset network hyperexcitability in presymptomatic Alzheimer's disease transgenic mice is suppressed by passive immunization with anti-human APP/Aβ antibody and by mGluR5 blockade. Front Aging Neurosci 9:1246. CrossRef

Lam AD, Deck G, Goldman A, Eskandar EN, Noebels J, Cole AJ (2017) Silent hippocampal seizures and spikes identified by foramen ovale electrodes in Alzheimer's disease. Nat Med 23:678–680. CrossRef

Lee MG, Hassani OK, Alonso A, Jones BE (2005) Cholinergic basal forebrain neurons burst with theta during waking and paradoxical sleep. J Neurosci 25:4365–4369. CrossRef Medline

Lee SH, Dan Y (2012) Neuromodulation of brain states. Neuron 76:209–222. CrossRef Medline

Louie K, Wilson MA (2001) Temporally structured replay of awake hippocampal ensemble activity during rapid eye movement sleep. Neuron 29:145–156. Medline

Lozsadi DA, Larner AJ (2006) Prevalence and causes of seizures at the time of diagnosis of probable Alzheimer's disease. Dement Geriatr Cogn Disord 22:121–124. CrossRef

Mander BA, Winer JR, Jagust WJ, Walker MP (2016) Sleep: a novel mechanistic pathway, biomarker, and treatment target in the pathology of Alzheimer's disease? Trends Neurosci 39:552–566. CrossRef Medline

Masuda A, Kobayashi Y, Kogo N, Saito T, Saido TC, Itohara S (2016) Cognitive deficits in single App knock-in mouse models. Neurobiol Learn Mem 135:73–82. CrossRef Medline

Minecan D, Natarajan A, Marzec M, Malow B (2002) Relationship of epileptic seizures to sleep stage and sleep depth. Sleep 25:899–904. Medline

Minkeviciene R, Rheims S, Dobszay MB, Zilberter M, Hartikainen J, Fülöp L, Penke B, Zilberter Y, Harkany T, Pitkänen A, Tanila H (2009) Amyloid beta-induced neuronal hyperexcitability triggers progressive epilepsy. J Neurosci 29:3453–3462. CrossRef Medline

Mitra P, Bokil H (2007) Observed brain dynamics. Oxford: Oxford University Press.

Mucke L, Masliah E, Yu G-Q, Mallory M, Rockenstein EM, Tatsuno G, Hu K, Kholodenko D, Johnson-Wood K, McConlogue L (2000) High-level neuronal expression of Aβ1–42 in wild-type human amyloid protein precursor transgenic mice: synaptotoxicity without plaque formation. J Neurosci 20:4050–4058. CrossRef

Musiek ES, Xiong DD, Holtzman DM (2015) Sleep, circadian rhythms, and the pathogenesis of Alzheimer disease. Exp Mol Med 47:e148. CrossRef Medline

Musiek ES, Bhimasani M, Zangrilli MA, Morris JC, Holtzman DM, Ju Y-ES (2018) Circadian rest-activity pattern changes in aging and preclinical Alzheimer disease. JAMA Neurol. Advance online publication. Retrieved May 3, 2018. CrossRef

Ng M, Pavlova M (2013) Why are seizures rare in rapid eye movement sleep? Review of the frequency of seizures in different sleep stages. Epilepsy Res Treat 2013:1–10. CrossRef

Pack AI, Galante RJ, Maislin G, Cater J, Metaxas D, Lu S, Zhang L, Smith Von R, Kay T, Lian J, Svenson K, Peters LL (2007) Novel method for high-throughput phenotyping of sleep in mice. Physiol Genomics 28:232–238. CrossRef

Palop JJ, Mucke L (2016) Network abnormalities and interneuron dysfunction in Alzheimer disease. Nat Rev Neurosci 17:777–792. CrossRef Medline

Palop JJ, Chin J, Roberson ED, Wang J, Thwin MT, Bien-Ly N, Yoo J, Ho KO, Yu G-Q, Kreitzer A, Finkbeiner S, Noebels JL, Mucke L

(2007) Aberrant excitatory neuronal activity and compensatory remodeling of inhibitory hippocampal circuits in mouse models of Alzheimer's disease. Neuron 55:697–711. CrossRef Medline

Patel V, Oh A, Voit A, Sultatos LG, Babu GJ, Wilson BA, Ho M, McArdle JJ (2014) Altered active zones, vesicle pools, nerve terminal conductivity, and morphology during experimental MuSK myasthenia gravis. PLoS One 9:e110571. CrossRef

Peter-Derex L, Yammine P, Bastuji H, Croisile B (2015) Sleep and Alzheimer's disease. Sleep Med Rev 19:29–38. CrossRef Medline

Pignatelli M, Lebreton F, Cho YH, Leinekugel X (2012) "Ectopic" theta oscillations and interictal activity during slow-wave state in the R6/1 mouse model of Huntington's disease. Neurobiol Dis 48:409–417. CrossRef

Quigg M (2000) Circadian rhythms: interactions with seizures and epilepsy. Epilepsy Res 42:43–45.

Quiroz YT, Budson AE, Celone K, Ruiz A, Newmark R, Castrillón G, Lopera F, Stern CE (2010) Hippocampal hyperactivation in presymptomatic familial Alzheimer's disease. Ann Neurol 68:865–875. CrossRef Medline

Rambli A, Abuzaid AHM, Bin Mohamed I, Hussin AG (2016) Procedure for detecting outliers in a circular regression model. PLoS One 11:e0153074. CrossRef Medline

Rasch B, Born J (2013) About sleep's role in memory. Physiol Rev 93:681–766. CrossRef Medline

Roh JH, Huang Y, Bero AW, Kasten T, Stewart FR, Bateman RJ, Holtzman DM (2012) Disruption of the sleep-wake cycle and diurnal fluctuation of β-amyloid in mice with Alzheimer's disease pathology. Sci Transl Med 4:150ra122. CrossRef

Rosenfeld C, Kousba A, Sultatos LG (2001) Interactions of rat brain acetylcholinesterase with the detergent Triton X-100 and the organophosphate paraoxon. Toxicol Sci 63:208–213. Medline

Saito T, Matsuba Y, Mihira N, Takano J, Nilsson P, Itohara S, Iwata N, Saido TC (2014) Single App knock-in mouse models of Alzheimer's disease. Nat Neurosci 17:661–663. CrossRef Medline

Sammaritano M, Gigli GL, Gotman J (1991) Interictal spiking during wakefulness and sleep and the localization of foci in temporal lobe epilepsy. Neurology 41:290–297. Medline

Sanchez PE, Zhu L, Verret L, Vossel KA, Orr AG, Cirrito JR, Devidze N, Ho K, Yu G-Q, Palop JJ, Mucke L (2012) Levetiracetam suppresses neuronal network dysfunction and reverses synaptic and cognitive deficits in an Alzheimer's disease model. Proc Natl Acad Sci USA 109:E2895–E2903. CrossRef

Sarkis RA, Dickerson BC, Cole AJ, Chemali ZN (2016) Clinical and neurophysiologic characteristics of unprovoked seizures in patients diagnosed with dementia. J Neuropsychiatry Clin Neurosci 28:56–61. CrossRef Medline

Scharfman HE (2012) Alzheimer's disease and epilepsy: insight from animal models. Future Neurol 7:177–192. CrossRef Medline

Sedigh-Sarvestani M, Thuku GI, Sunderam S, Parkar A, Weinstein SL, Schiff SJ, Gluckman BJ (2014) Rapid eye movement sleep and hippocampal theta oscillations precede seizure onset in the tetanus toxin model of temporal lobe epilepsy. J Neurosci 34:1105–1114. CrossRef Medline

Sedigh-Sarvestani M, Blumenfeld H, Loddenkemper T, Bateman LM (2015) Seizures and brain regulatory systems: consciousness, sleep, and autonomic systems. J Clin Neurophysiol 32:188–193. CrossRef Medline

Shankar GM, Leissring MA, Adame A, Sun X, Spooner E, Masliah E, Selkoe DJ, Lemere CA, Walsh DM (2009) Biochemical and immunohistochemical analysis of an Alzheimer's disease mouse model reveals the presence of multiple cerebral Aβ assembly forms throughout life. Neurobiol Dis 36:293–302. CrossRef Medline

Shouse MN, Farber PR, Staba RJ (2000) Physiological basis: how NREM sleep components can promote and REM sleep compo-nents can suppress seizure discharge propagation. Clin Neurophysiol 111:S9–S18. CrossRef

Skaggs WE, McNaughton BL (1996) Replay of neuronal firing sequences in rat hippocampus during sleep following spatial experience. Science 271:1870–1873. Medline

Sterniczuk R, Dyck RH, LaFerla FM, Antle MC (2010) Characterization of the 3xTg-AD mouse model of Alzheimer's disease: part 1. Circadian changes. Brain Res 1348:139–148. CrossRef Medline

Šišková Z, Justus D, Kaneko H, Friedrichs D, Henneberg N, Beutel T, Pitsch J, Schoch S, Becker A, Kammer von der H, Remy S (2014) Dendritic structural degeneration is functionally linked to cellular hyperexcitability in a mouse model of Alzheimer's disease. Neuron 84:1023–1033. CrossRef

Van Dort CJ, Zachs DP, Kenny JD, Zheng S, Goldblum RR, Gelwan NA, Ramos DM, Nolan MA, Wang K, Weng F-J, Lin Y, Wilson MA, Brown EN (2015) Optogenetic activation of cholinergic neurons in the PPT or LDT induces REM sleep. Proc Natl Acad Sci USA 112:584–589. CrossRef Medline

Vazquez J, Baghdoyan HA (2001) Basal forebrain acetylcholine release during REM sleep is significantly greater than during waking. Am J Physiol 280:R598–R601. CrossRef

Vitiello MV, Bokan JA, Kukull WA, Muniz RL, Smallwood RG, Prinz PN (1984) Rapid eye movement sleep measures of Alzheimer's-type dementia patients and optimally healthy aged individuals. Biol Psychiatry 19:721–734.

Vloeberghs E, Van Dam D, Engelborghs S, Nagels G, Staufenbiel M, De Deyn PP (2004) Altered circadian locomotor activity in APP23 mice: a model for BPSD disturbances. Eur J Neurosci 20:2757–2766. CrossRef Medline

Vossel KA, Beagle AJ, Rabinovici GD, Mucke L (2013) Seizures and epileptiform activity in the early stages of Alzheimer disease. JAMA Neurol 70:1158–1166. CrossRef Medline

Vossel KA, Ranasinghe KG, Beagle AJ, Mizuiri D, Honma SM, Dowling AF, Darwish SM, Van Berlo V, Barnes DE, Mantle M, Karydas AM, Coppola G, Roberson ED, Miller BL, Garcia PA, Kirsch HE, Mucke L, Nagarajan SS (2016) Incidence and impact of subclinical epileptiform activity in Alzheimer's disease. Ann Neurol 80:858–870. CrossRef

Wickham H (2009) ggplot2: elegant graphics for data analysis. New York: Springer.

Wickham H, Francois R (2015) dplyr: a grammar of data manipulation. R Package. Available at: http://CRAN.R-project.org/package=dplyr.

Wilensky AE, Schafe GE, LeDoux JE (2000) The amygdala modulates memory consolidation of fear-motivated inhibitory avoidance learning but not classical fear conditioning. J Neurosci 20:7059–7066. CrossRef

Wisor JP, Edgar DM, Yesavage J, Ryan HS, McCormick CM, Lapustea N, Murphy GM (2005) Sleep and circadian abnormalities in a transgenic mouse model of Alzheimer's disease: a role for cholinergic transmission. Neuroscience 131:375–385. CrossRef

Wu JW, Hussaini SA, Bastille IM, Rodriguez GA, Mrejeru A, Rilett K, Sanders DW, Cook C, Fu H, Boonen RACM, Herman M, Nahmani E, Emrani S, Figueroa YH, Diamond MI, Clelland CL, Wray S, Duff KE (2016) Neuronal activity enhances tau propagation and tau pathology in vivo. Nat Neurosci 19:1085–1092. CrossRef

Xu W, Fitzgerald S, Nixon RA, Levy E, Wilson DA (2015) Early hyperactivity in lateral entorhinal cortex is associated with elevated levels of AβPP metabolites in the Tg2576 mouse model of Alzheimer's disease. Exp Neurol 264:82–91. CrossRef Medline

Yuan P, Grutzendler J (2016) Attenuation of -amyloid deposition and neurotoxicity by chemogenetic modulation of neural activity. J Neurosci 36:632–641. CrossRef Medline

Zhang L (2011) Voluntary oral administration of drugs in mice. Protoc Exch. CrossRef